microbial biotechnology

Open Access

Engineering siderophore production in *Pseudomonas* to improve asbestos weathering

Marion Lemare,[1,†] Hélène Puja,[1,†] Sébastien R. David,[1] Sébastien Mathieu,[1] Dris Ihiawakrim,[2] Valérie A. Geoffroy[1,*] and Coraline Rigouin[1,]**

[1] *Université de Strasbourg, CNRS-UMR7242, BSC, ESBS, 300 Bld Sébastien Brant, 67413, Illkirch, Strasbourg, France.*

[2] *Université de Strasbourg, CNRS-UMR7504, IPCMS, 23 Rue du Loess, BP, 43, 67034, Strasbourg, France.*

Summary

Iron plays a key role in microbial metabolism and bacteria have developed multiple siderophore-driven mechanisms due to its poor bioavailability for organisms in the environment. Iron-bearing minerals generally serve as a nutrient source to sustain bacterial growth after bioweathering. Siderophores are high-affinity ferric iron chelators, of which the biosynthesis is tightly regulated by the presence of iron. Pyoverdine-producing *Pseudomonas* have shown their ability to extract iron and magnesium from asbestos waste as nutrients. However, such bioweathering is rapidly limited due to repression of the pyoverdine pathway and the low bacterial requirement for iron. We developed a metabolically engineered strain of *Pseudomonas aeruginosa* for which pyoverdine production was no longer repressed by iron as a proof of concept. We compared siderophore-promoted dissolution of flocking asbestos waste by this optimized strain to that by the wild-type strain. Interestingly, pyoverdine production by the optimized strain was seven times higher in the presence of asbestos waste and the dissolution of magnesium and iron from the chrysotile fibres contained in flocking asbestos waste was significantly enhanced. This innovative mineral weathering process contributes to remove toxic iron from the asbestos fibres and may contribute to the development of an eco-friendly method to manage asbestos waste.

Received 2 October, 2021; accepted 25 May, 2022.
For correspondence. *E-mail valerie.geoffroy@unistra.fr.
**E-mail rigouin@unistra.fr; Tel: +33 (0)3 68 85 48 20.
†These two authors contributed equally to this work.
Microbial Biotechnology (2022) **15**(9), 2351–2363
doi:10.1111/1751-7915.14099
Funding Information
This work has been conducted under the framework of the IdEx Unistra supported by the Investments for the future programme of the French Government and partially funded by the agence nationale de la Recherche.

Introduction

In an aerobic environment at neutral pH, iron is poorly bioavailable, yet it is an important metal for microorganisms. In most natural habitats, iron, in its oxidized state (Fe^{3+}), forms stable ferric oxide hydrate complexes, lowering its solubility. As a consequence, soluble iron concentrations generally vary between 10^{-9} and 10^{-18} M (Miethke and Marahiel, 2007) while bacteria require between 10^{-5} and 10^{-7} M (Khan *et al.*, 2018) for their optimal growth. The main strategy developed by many organisms to access iron is the production of siderophores. Indeed, iron is an important nutrient involved as a cofactor of many bacterial enzymes and the redox properties of the metal are essential for many cellular processes. The response to iron must be tightly controlled by the cell, as excessive concentrations of intracellular iron may lead to oxidative stress (Andrews *et al.*, 2003). In this context, siderophores are key players in bacterial iron homeostasis (Cornelis *et al.*, 2011; Schalk *et al.*, 2011).

Siderophores can be classified into three groups based on the chemical nature of their chelating groups: catechol-type siderophores, hydroxamate-type siderophores and mixed-type siderophores (α-hydroxycarboxylate and 2-(2-hydroxyphenyl-oxazoline) (Ahmed and Holmström, 2014). More than 500 siderophores have been described and most of them have a peptide backbone and harbour functional groups that donate the oxygen ligands for Fe^{3+} coordination (Boukhalfa and Crumbliss, 2002). The affinity of siderophores for Fe^{3+} is high, varying from 10^{23} to 10^{52} M^{-1}, and they have been reported to also complex with other metals (*e.g.* Cu, Cd, Ni, Co, Zn, Al and Mn), macronutrients and radionuclides (Chen *et al.*, 1994; Braud *et al.*, 2010; Johnstone and Nolan, 2015; Williamson *et al.*, 2021).

Upon iron starvation, these secondary metabolites are synthesized in the cytoplasm and secreted into the medium where they chelate Fe^{3+}. The iron-complexed siderophore is then taken up *via* selective transport mechanisms involving TonB-dependant membrane receptors or membrane-associated reductase activity to

deliver the iron inside the cell (Gasser *et al*., 2015; Ringel *et al*., 2018; Josts *et al*., 2021). Once in the cell, both the siderophore and iron trigger various signalling pathways, allowing adaptation of the cell to the iron concentration, the ability to respond to oxidative stress and virulence (Khan *et al*., 2018). Ultimately, siderophores play an important role in infection for pathogenic bacteria such as *Pseudomonas aeruginosa, Escherichia coli* or *Salmonella typhimurium* (Holden and Bachman, 2015). In the environment, siderophores produced by soil microorganisms participate in plant growth, the weathering of soil minerals and the biogeochemical cycling of iron (Kraemer, 2004; Ahmed and Holmström, 2014; Aznar and Dellagi, 2015).

As a result of these properties, siderophores have been used in biotechnology in many fields (Saha *et al*., 2016; Serrano, 2017; Albelda-Berenguer *et al*., 2019). In medicine, the chelating properties of siderophores are used to treat iron-overload disease (Hatzipantelis *et al*., 2014) and are exploited in bioimaging, biosensing and diagnosis (Petrik *et al*., 2017; Nosrati *et al*., 2018; Tonziello *et al*., 2019). In addition, their ability to cross bacterial membranes using specific transporters has led to the synthesis of siderophore-antibiotic conjugates that are able to hijack the iron-acquisition pathway to deliver antibiotics inside the cell (Mislin and Schalk, 2014; Saisho *et al*., 2018; Schalk, 2018). In agriculture, siderophores are used to promote plant growth (Serrano, 2017), as pathogen biocontrol agents (Gull and Hafeez, 2012) and in soil bioremediation for bioleaching (Williamson *et al*., 2021) or bioweathering (Ferret *et al*., 2014; David, *et al*., 2020b).

Recently, our group demonstrated the role of siderophores and siderophore-producing bacteria in asbestos weathering (David, *et al*., 2020a; David, *et al*., 2020b, 2020c). Asbestos is an industrial term for naturally occurring fibrous silicate minerals belonging to serpentine or amphibole groups. These minerals were widely used for 30 years due to their insulating, chemical and mechanical properties. Chrysotile, the single mineral species from the serpentine group, represents 95% of world production (Kanarek, 2011). Chrysotile is a hydrated magnesium silicate with the theoretical composition $Mg_3Si_2O_5(OH)_4$. Its structure consists of a double layer made of an inner silicate layer and an outer magnesium hydroxide layer (brucite), in which the Si and Mg can be replaced by Fe^{3+} and Fe^{2+} respectively (Virta, 2002). However, exposure to asbestos fibres can cause serious health problems, such as fibrogenesis of the lung, pleural calcification, mesothelioma and ovarian or digestive system cancers (Scherpereel, 2016; Fiche toxicologique amiante, 2018). The toxicity of asbestos is partially due to the presence of iron in the inhaled fibres, which induces when dissolved the production of free radicals, causing DNA damage (Pascolo *et al*., 2013; Valko *et al*., 2016). Consequently, asbestos has been banned in many countries, generating a vast amount of asbestos-containing waste. Currently, most asbestos waste is typically disposed of in controlled landfill sites, although the toxicity and potential health and environmental risk of asbestos fibres remain (Spasiano and Pirozzi, 2017; Paolini *et al*., 2019). Because these minerals can represent an efficient source of nutrients for bacteria (David, *et al*., 2020a; David, *et al*., 2020c), the biological dissolution of asbestos fibres represents a tremendous opportunity to meet the demand for the eco-friendly management of asbestos wastes (Wallis *et al*., 2020).

Microorganisms, such as filamentous fungi (Daghino *et al*., 2006), rhizospheric bacteria (Rajkumar *et al*., 2009) and Gram-positive bacteria (Bhattacharya *et al*., 2016) have a common siderophore-driven mechanism to access iron from asbestos. Recently, David *et al*. (2020a; 2020c) showed the involvement of the bacterial siderophores produced by *Pseudomonas aeruginosa* in iron depletion from raw asbestos and wastes, such as flocking asbestos waste (FAW) and asbestos cement waste (ACW). The dissolution of the brucite layer, which potentially supplies Mg and/or Fe, was shown to be sufficient to sustain bacterial growth, confirming that asbestos minerals represent a bacterial nutrient source. Pyoverdine (PVD) is the main siderophore produced by *P. aeruginosa* (Budzikiewicz, 1997). More than a hundred structures of PVD has been described (Fuchs *et al*., 2001; Meyer *et al*., 2008) and several can efficiently dissolve iron from raw asbestos (David, *et al*., 2020c), as well as asbestos waste (David, *et al*., 2020a). In *Pseudomonas*, the biosynthesis of PVD is tightly regulated and directly dependent on the absence of iron (Schalk *et al*., 2020). The ferric uptake regulator (Fur) is the main regulator involved in PVD synthesis. Under iron-rich conditions, Fur binds to the promoter–operator region, a specific region of 19 bp located in between the −35 and − 10 regions of the promoter called Fur box and inhibits the transcription of the corresponding genes (Pohl *et al*., 2003; Hassan and Troxell, 2013). One of the Fur-controlled genes is *pvdS*, an extracytoplasmic sigma factor required for the transcription of a number of PVD-biosynthetic genes (Leoni *et al*., 2000). Due to such regulation, PVD production stops when a sufficient intracellular concentration of iron is reached, preventing the potential toxicity of high iron concentration.

When growing in an iron-depleted medium in the presence of the mineral, *P. aeruginosa* PAO1 synthesizes PVD, which dissolves the metal from the fibres. However, as the iron concentration increases, siderophore synthesis is repressed, thus preventing any further metal dissolution. Consequently, we hypothesized that the siderophore must be produced continuously for efficient

dissolution. Here, we describe the engineering of *P. aeruginosa* (PaM1) as a model to produce PVD independently of the iron concentration. We quantified the PVD production of this iron-independent siderophore-producing mutant and the effect of over-expression of the PvdS transcriptional regulator on two PVD biosynthetic genes, *pvdD* and *pvdA*, as representatives of the induction of the PVD pathway. This bioengineered strain demonstrates the potential of the PVD-weathering process on FAW, one of the most representative forms of asbestos waste. This anthropogenic material is mostly composed of chrysotile fibres (David, *et al*., 2020a) combined with a gypsum matrix, widely used for insulation in buildings. After the biological treatment of FAW, the amount of extracted iron and magnesium are measured as markers of fibre dissolution, together with the resulting fibre composition. We highlight how the regulation of PVD can be modulated to better fit with an efficient eco-process to remove the toxicity of asbestos fibres. This biotechnological advance should make it possible to avoid the continuing disposal of asbestos waste in landfills, which is the common practice today, and to consequently reduce this environmental problem. Given the major public health problem of asbestos and the lack of satisfactory treatment, our findings could have a significant societal impact.

Results

PaM1 produces pyoverdine in the presence of iron

To obtain a PVD production independent of iron, we built the mutant strain PaM1 in which the native Fur-box promoter region of *pvdS* is replaced by the arabinose-inducible promoter. The growth and PVD production of both the wild-type (PAO1) and mutant (PaM1) strains were then assessed. The presence of arabinose in the medium did not influence the growth of PAO1 and PaM1 (Fig. S1). On the contrary, the iron concentration clearly affected bacterial growth, with optimal growth obtained with 5 μM $FeCl_3$ (Fig. S2). We compared the PVD production of the two strains by analysing the amount of PVD relative to bacterial growth. PVD production was high for PAO1 when the iron concentration was <50 nM and decreased as the iron concentration increased (Fig. 1A), in accordance with the regulation of PVD being dependent on the absence of iron. By contrast, PVD production by PaM1 was low regardless of the iron concentration. We next assessed PVD production by PAO1 and PaM1 in increasing concentrations of arabinose (0 to 0.5%) (Fig. 1B). PVD production by PAO1 did not change, irrespective of the concentration of arabinose in the absence of iron. By contrast, PVD production by PaM1 significantly increased as the concentration of arabinose increased from 0.01% to 0.5%. Higher concentrations of arabinose (0.5 to 2%) were tested but did not significantly improve PVD production (data not shown). These experiments allowed us to determine an optimal concentration of arabinose for PVD production of 0.5%. Overall, these results show that PVD production by PaM1 is independent of iron and relies solely on the arabinose inducer in a dose-dependent manner.

To estimate the amount of PVD produced in optimal conditions for PaM1 and PAO1, strains were grown in rich or minimal medium, supplemented or not with 0.5% arabinose and/or 5 μM $FeCl_3$ (Fig. 2). In rich medium, the total amount of PVD measured for PAO1 was low (143 ± 12 mg l^{-1}) due to the presence of iron in the medium, whereas that for PaM1 reached 574 ± 10 mg l^{-1} when induced by arabinose. In minimal medium, the highest production was obtained for both strains in the iron-depleted and arabinose-supplemented condition: PAO1 produced 529 ± 9 mg l^{-1} and PaM1 574 ± 4 mg l^{-1}. Overall, these results show that PaM1 can produce a high amount of PVD in both rich and minimal media. In addition, our data show that the arabinose-dependent PVD production of PaM1 is not significantly different from that of PAO1 under conditions of iron restriction.

Transcription of pvdS *increases in PaM1 following arabinose induction*

We first assessed *pvdS* transcript levels in PaM1 and in PAO1 relative to that of PAO1 in *pvdS*-repressed condition (CAA with iron) (Fig. 3A). In PAO1, the level of *pvdS* transcripts was 123-fold higher in the absence of iron than in its presence. For PaM1 without arabinose, the level of *pvdS* transcripts was higher than that of repressed PAO1, suggesting leakage in the induction system. The addition of 0.5% arabinose triggered an increase in the level of *pvdS* transcripts in PaM1 by ≃ 1100-fold, which was significantly higher than in PAO1 in the absence of iron. Of note, controls showed that the exposure of PAO1 to arabinose or PaM1 to iron had no significant impact on the level of *pvdS* transcripts. This strongly shows that modification of the regulation of *pvdS* transcription in PaM1 allows the overproduction of transcripts in the presence of the arabinose inducer.

We then monitored the transcription of *pvdD* and *pvdA* (Fig. 3B and C respectively), two genes under the control of PvdS and involved in PVD biosynthesis. We measured a ≃ 250-fold increase in *pvdD* transcript levels for PaM1 when *pvdS* was induced by arabinose, with no significant difference relative to the number of *pvdS* transcripts in PAO1 under induced conditions. We observed the same tendency for *pvdA* transcription, for which there was no significant increase in *pvdA* transcript levels in PaM1 relative to PAO1 under induced

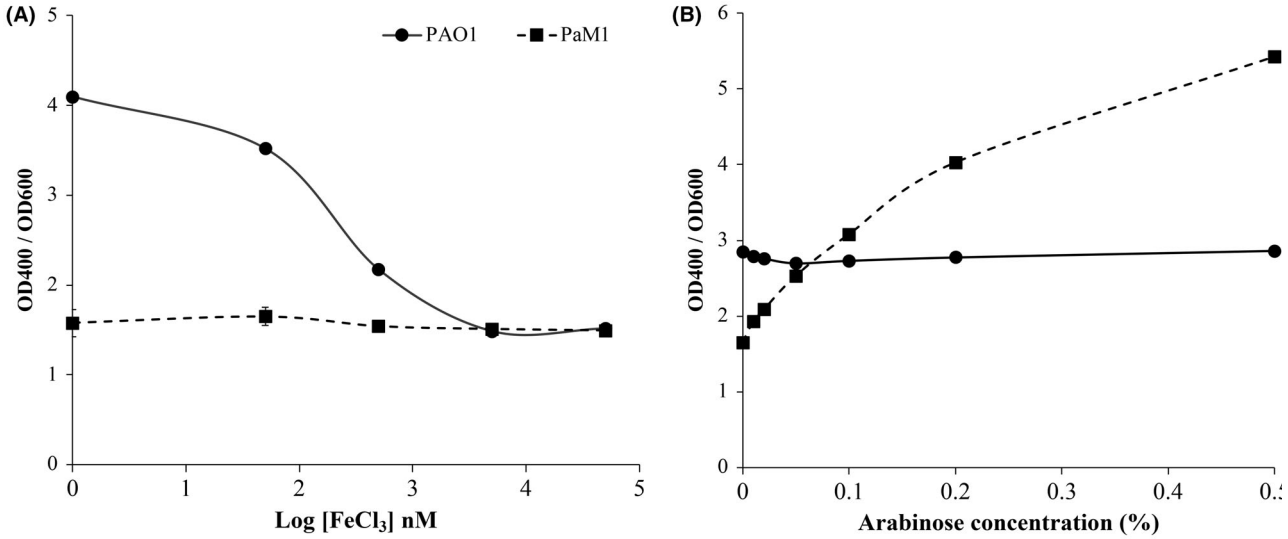

Fig. 1. Pyoverdine production relative to growth (OD400/OD600) after 9 h of incubation at 30°C for the strains *P. aeruginosa* PAO1 (solid line) and PaM1 (dashed line) depending on iron concentration (nM) (A) or arabinose concentration (% v/v) (B).

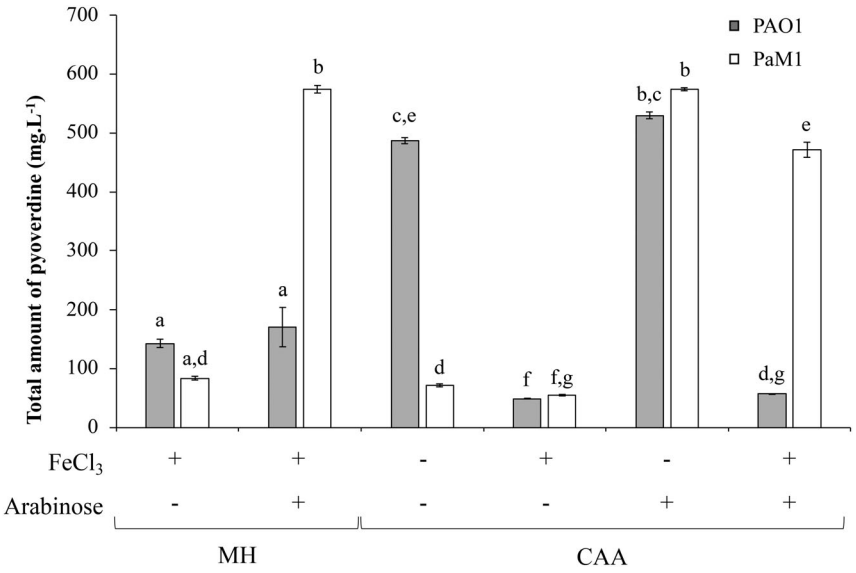

Fig. 2. Pyoverdine production of *P. aeruginosa* strains PAO1 (grey bars) and PaM1 (white bars) assessed after 24 h of growth in rich (MH) or minimal (CAA) medium supplemented or not with iron (5 μM FeCl3) and/or arabinose (0.5%). Error bars indicate the standard error over mean of triplicates experiments. Kruskal–Wallis non-parametric test was used to calculate statistically significant differences. Letters (a to g) above the bars represent the result of the test: bars harbouring the same letter(s) are not statistically different ($P \geq 0.05$).

conditions (with arabinose and without iron respectively). Overall, these results show that although more *pvdS* transcripts are generated, the expression of genes under its control does not increase accordingly.

Pyoverdine production by PaM1 increases in the presence of asbestos waste

We evaluated the efficiency of the asbestos waste weathering by growing both PAO1 and PaM1 in the presence of FAW. The bacterial cell number after each cycle of incubation was significantly higher in the presence of FAW for PAO1 and PaM1 (Fig. 4). The growth was even higher when the cells were grown in Mg-supplemented CAA medium (data not shown). These results confirm the previous observations of David *et al.* (2020a) and prove that the stimulation of bacterial growth is due to the dissolution of nutrients from the fibres (release of iron and magnesium from the fibres). The monitoring of PVD produced by the two strains after

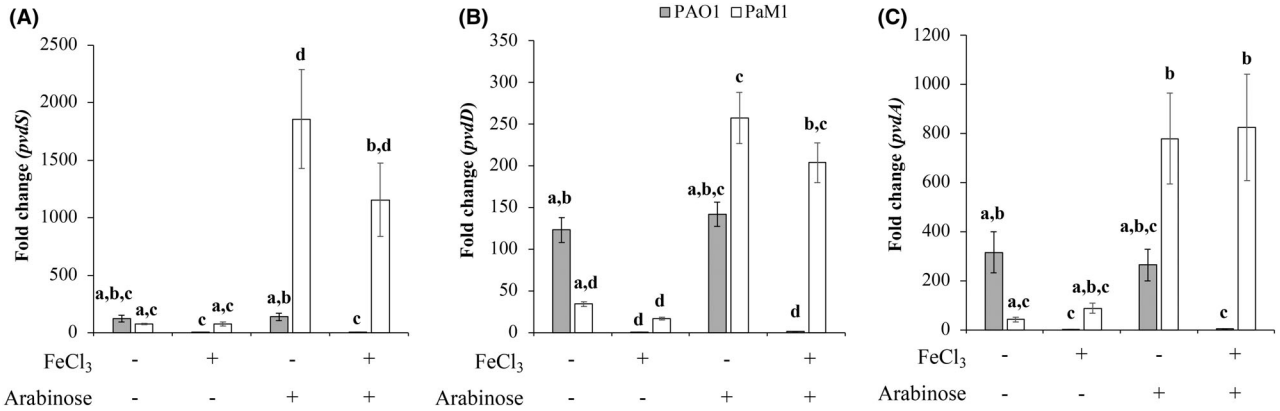

Fig. 3. Relative transcript levels of genes involved in pyoverdine biosynthesis for *P. aeruginosa* strains PAO1 (grey bars) and PaM1 (white bars). Transcript level of pvdS (A), pvdD (B) and pvdA (C) relative to the levels measured in PAO1 grown in CAA + FeCl3 are shown. Error bars indicate the standard error over mean of triplicates experiments. Kruskal–Wallis non-parametric test was used to calculate statistically significant differences. Letters (a to d) above the bars represent the result of the test: bars harbouring the same letter(s) are not statistically different ($P \geq 0.05$).

each growth cycle showed its production by PAO1 to be low in CAA(-Mg) (<5 mg·L^{-1}) and to increase to ≃ 40 mg·L^{-1} in the presence of FAW (Fig. 5). This difference can be explained by the stimulation of growth in the presence of FAW, leading to a global increase in PVD production. The observed weak PVD synthesis by PAO1 is due to the repression exerted by the dissolved iron from asbestos. Interestingly, the amount of PVD produced by PaM1 was significantly higher than that by PAO1, independently of the presence of FAW (Fig. 5). This difference cannot be due to differences in growth, as both strains grew equally (Fig. 4 and S3). Moreover, PVD production by PaM1 was elevated for each cycle, unlike that of PAO1 which remained close to the detection limit. In the presence of FAW, PVD production by PaM1 was high during the first two cycles and reached 523 ± 23 mg·L^{-1} at cycle 2 and then gradually decreased with the number of cycles. Overall, PVD production by PaM1 at the end of the five cycles was ≃ 7-fold higher than the wild-type strain, even though the number of cells at the end of each growth cycle was equivalent between the two strains.

Enhancement of iron and magnesium dissolution from asbestos waste by PaM1

We measured the amount of magnesium and iron in both the supernatant and cells to estimate the dissolution of iron and magnesium from the fibres at the end of each growth cycle (Fig. 6). Overall, the amount of iron

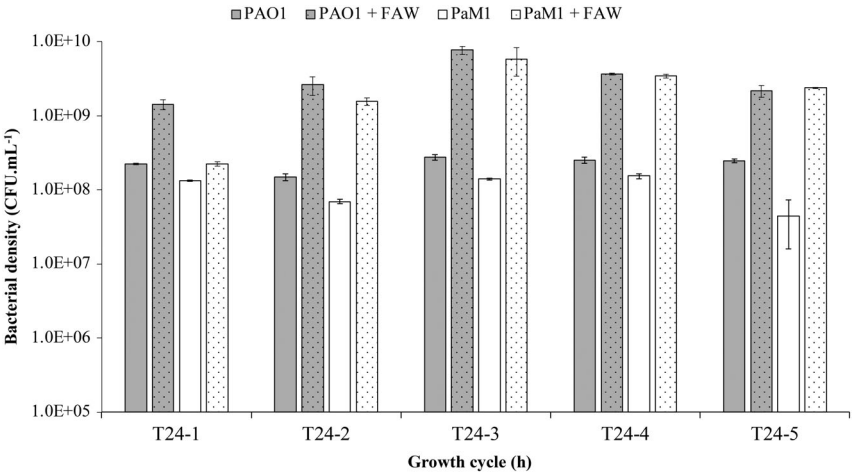

Fig. 4. Numeration of *P. aeruginosa* strains PAO1 (grey bars) and PaM1 (white bars). The number of cells (CFU ml^{-1}) was assessed during five growth cycles of 24 h (T24-1 to T24-5) in CAA medium without magnesium CAA(-Mg) supplemented with arabinose, in the presence (dots) or absence (plain) of flocking asbestos wastes. Error bars indicate the standard errors of the means of three biological replicates.

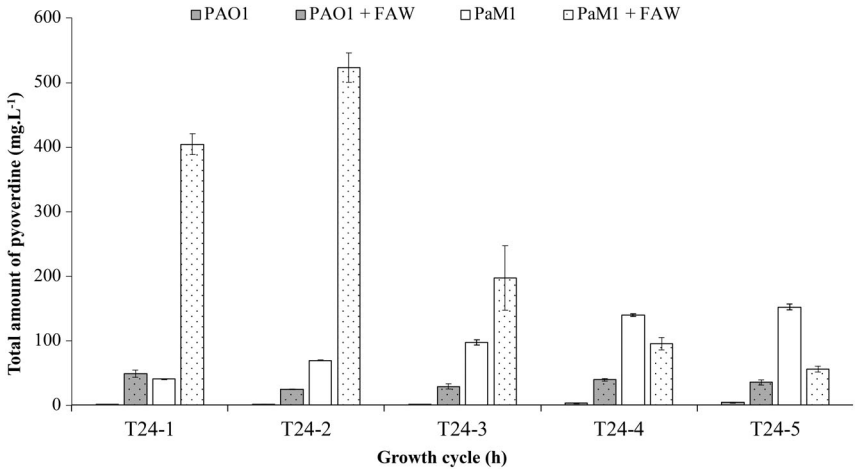

Fig. 5. Pyoverdine production of *P. aeruginosa* strains PAO1 (grey bars) and PaM1 (white bars). The concentration of pyoverdine (mg l^{-1}) was assessed during five growth cycles of 24 h (T24-1 to T24-5) in CAA medium without magnesium CAA(-Mg) supplemented with arabinose (1%), in the presence (dots) or absence (plain) of flocking asbestos wastes. Error bars indicate the standard errors of the means of three biological replicates.

and magnesium dissolved from FAW was higher for PaM1 than PAO1. The highest level of extraction was measured for cycles 1 and 2 for magnesium and cycles 2 and 3 for iron, suggesting that the extraction begins with magnesium. In addition, iron and magnesium mainly accumulated in the supernatant, particularly during the early cycles for PaM1. After cycle 5, although the amount of iron and magnesium measured was significantly lower, both elements were still extracted, suggesting that additional cycles could favour further extraction. Overall, a total of 64 ± 8 μg of iron was extracted from FAW by PAO1 and 100 ± 10 μg by PaM1 after five cycles, representing an extraction of 7.0 ± 0.9% and 10.9 ± 1.1% respectively. Concerning magnesium, 534 ± 128 μg was extracted from FAW by PAO1 and 1004 ± 125 μg by PaM1, representing an extraction of 3.6 ± 0.9% and 6.8 ± 0.8% respectively. In conclusion, PaM1 can extract significantly more iron and magnesium from FAW fibres than PAO1.

Analysis by STEM-EDX of the chrysotile fibres after the short-term weathering of FAW showed the iron composition in almost all fibre areas to be <1% (Fig. S4A–F). We measured a lower mass % of iron after alteration by PaM1 than by PAO1 (0.9% and 1.3% respectively), confirming a higher iron extraction by the mutant strain (Fig. S4E). Furthermore, the percentage of iron could be extremely low, close to zero, especially at the end of the fibres. The Fe/Si atomic ratio showed the same trend, with 0.029 (PAO1) versus 0.022 (PaM1), confirming the active dissolution of iron driven by the bacteria (Fig. S4F). Moreover, we observed a greater decrease in silicon content after alteration by PaM1 (40.29%) than by PAO1 (43.62%) (Fig. S4E), suggesting that silicon dissolution from asbestos fibres may be another reliable marker for bacterial weathering.

Discussion

Here, we describe the modification of the regulation of PVD production in *Pseudomonas aeruginosa* to improve asbestos weathering. Replacement of the iron-responsive promoter region of *pvdS* by an inducible promoter rendered the production of PVD dependent on solely the inducer. We chose to use the AraC/pBAD promoter because it is widely used for the controlled expression of proteins in several microorganisms (Balzer *et al.*, 2013), in particular, *Pseudomonas aeruginosa* (Qiu *et al.*, 2008; Huse *et al.*, 2013; Pasqua *et al.*, 2017). The use of this promoter is this relevant to establish the proof of concept that PVD production can be modulated by a stimulus other than iron. Other types of promoters, such as constitutive promoters, are worth trying (Zobel *et al.*, 2015; Elmore *et al.*, 2017) to prevent (i) the perturbation of metabolism that inducers such as arabinose may have on the strain and (ii) excessive cost if the process is transferred to a larger scale. In our study, the measurement of *pvdS* transcript levels in the engineered strain PaM1 provides evidence that AraC/pBAD works efficiently in *P. aeruginosa*. We obtained higher levels of *pvdS* transcripts in PaM1 upon induction with 0.5% arabinose than in PAO1 under iron depletion. The difference can be attributed to the strong repression of *pvdS* exerted by the entry of iron into the cell resulting from PVD production in PAO1, whereas no repression occurs in PaM1, allowing a constant increase in transcript levels during growth. However, although *pvdS* transcript levels were higher, we did not measure a

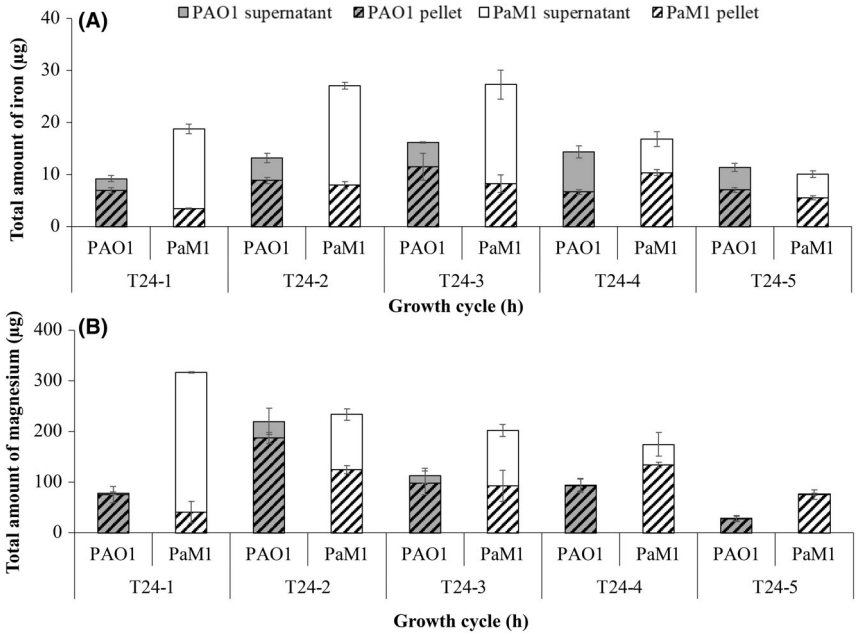

Fig. 6. Amount of iron (A) and magnesium (B) extracted from raw asbestos waste by *P. aeruginosa* strains PAO1 (grey bars) and PaM1 (white bars). The quantity of iron and magnesium (µg) was assessed during five growth cycles of 24 h (T24-1 to T24-5) in CAA medium without magnesium CAA(-Mg) supplemented with arabinose, in the presence of flocking asbestos wastes. Elements were measured in the bacterial cells (pellet, dashed) and supernatant (plain). Error bars indicate the standard errors of the means of three biological replicates.

corresponding increase in the transcription of the *pvdD* or *pvdA* genes, of which the transcription relies on *pvdS*. As a consequence, the amount of PVD produced by PaM1 was not significantly higher than that for PAO1 under these conditions. This highlights the fact that the efficiency of PVD synthesis is likely already optimal in PAO1 under iron-depleted conditions.

Our data provide evidence that overproduction of the sigma factor PvdS does not impair *P. aeruginosa* growth. Of note, as PvdS controls the transcription of several virulence factors (Ochsner *et al.*, 1996; Wilderman *et al.*, 2001), its overproduction may have an impact on PAO1 behaviour under conditions of infection. In this study, we focused on the model strain PAO1 because it showed the best asbestos weathering in our previous study (David, *et al.*, 2020b). However, the use of an opportunistic pathogen is not suitable for developing an innocuous process to manage untreated asbestos waste. We are currently implementing the strategy using a non-pathogenic *Pseudomonas* species, such as *P. putida*, of which PVD biosynthesis is also under the Fur repressor (Venturi *et al.*, 1995). *P. putida* has been used as a chassis strain for the production of recombinant proteins and polymers (Nikel *et al.*, 2016) and has been widely used in bioremediation strategies (Kahlon, 2016). Although the regulation of PVD synthesis has not been completely described, pvdS transcription has been engineered and has led to the constitutive production of PVD (Becker *et al.*, 2018). Whether PVD production in *P. putida* can lead to efficient asbestos weathering is under assessment.

We tested the hypothesis that iron-independent PVD production can improve metal dissolution from asbestos fibres by growing the engineered PaM1 strain in the presence of one of the most representative forms of asbestos waste: FAW. First, our work confirms that FAW stimulates the growth of *Pseudomonas* strains through iron and Mg dissolution from the fibres, as already described by David et *al.* (2020a). The level of these elements in asbestos is several thousand times higher (personal data) than that required by *Pseudomonas aeruginosa* for optimal growth (56 µg l^{-1} Fe^{3+} and 200 µg l^{-1} Mg^{2+}) (Heldal *et al.*, 1985; Groisman *et al.*, 2013). This gap between metal availability and requirement suggests that multiplication of the bacteria may not be sufficient to dissolve all the magnesium and iron contained in the fibres, as the wild-type strain will not accumulate these elements beyond their potential toxic levels. Thus, the use of metabolic engineering strategies to modify bacterial metal homeostasis can lead to an improvement in the extraction performance of the bacteria (Diep *et al.*, 2018). In *Pseudomonas*, Mg^{2+} uptake takes place via activation of the PhoP/PhoQ two component system in Mg^{2+}-limiting environments and such passive transport occurs mainly via porins (McPhee *et al.*, 2006). There is no evidence that PVD can chelate Mg^{2+}. Therefore, we previously hypothesized that Mg^{2+} is dissolved when the fibres are introduced into aqueous

solution (David, *et al*., 2020a). Mg^{2+} dissolution could be the first step of alteration of the fibres and may trigger weakening of the fibre structure, facilitating access of the PVD to the deeper iron-containing layers. Iron uptake, however, involves active transporters and requires the production of siderophores (Cunrath *et al*., 2016). Iron extraction may thus constitute the second step of the alteration, promoting further destructuration of the fibre, thus allowing more magnesium dissolution and iron extraction. Our data with the mutant PaM1 support this hypothesis, as the enhancement of PVD production directly correlated with an increase in both iron and magnesium dissolution (Fig. 6).

When PaM1 was grown in the presence of arabinose and FAW, the production of PVD was almost seven times higher than that of PAO1. This higher PVD concentration led, however, to only a two-fold increase in iron and magnesium extraction. This implies that all the PVD is not involved in Fe^{3+} chelation. Indeed, we estimated that only 23% (for PAO1) and 12% (for PaM1) of PVD is complexed with iron. This suggests that either PVD is complexed to another metal or that the iron contained in the fibres is not accessible to PVD (because of the structure of the fibres or because of PVD adsorption to the fibres). Indeed, PVD can be adsorbed onto the surface of iron-bearing minerals, such as metal oxides (Upritchard *et al*., 2007) or smectite (Ferret *et al*., 2014), which may lead to modification of the surface structure. Although arabinose stimulated the production of PVD from PaM1 in the first two growth cycles, our results showed a decrease of PVD in solution from cycles 2 to 5, together with a decrease in magnesium and iron extraction. Changes in fibre morphology may lead to lower availability of iron to PVD, explaining this tendency. Another hypothesis to explain such a decrease could be the formation of a biofilm on the asbestos fibres after a few cycles. *P. aeruginosa* is a biofilm-forming bacteria that produces exopolysaccharides (EPS) responsible for iron sequestration by PVD trapped in this matrix. Such interface could constitute a barrier to deterioration, both by the presence of EPS, which creates a physical barrier between the fibre and the solution, and by the nature of the EPS, which has the property of complexing with the dissolved elements. Such phenomena have been observed during the alteration of bottom ash by *Pseudomonas*, in which the establishment of a biofilm reduced the rate of alteration (Aouad *et al*., 2008). Whether this is the case with *P. aeruginosa* grown with FAW has yet to be determined.

Finally, we show that the improvement in iron extraction by PVD is not toxic for the bacteria. Our data provide evidence that iron does not accumulate in the cell but rather in the external medium. As high iron concentrations are toxic for the cell, protection from internal toxic iron concentrations by the regulator Fur persists, even in PaM1, in which the main iron acquisition system (PVD) is overexpressed. Of note, aside from PVD, the second endogenous siderophore, pyochelin (PCH), has already been shown to be involved in asbestos–iron dissolution (David, *et al*., 2020c), as well as that of organic acids (Mohanty *et al*., 2018). Indeed, it has been reported that *P. aeruginosa* in iron-containing medium produces more PCH than PVD (Cunrath *et al*., 2016). The role of PCH in iron extraction by PAO1 and PaM1 in the presence of FAW has yet to be assessed but may be another pathway to explore and engineer to enhance the alteration of asbestos fibres. In this context, transcriptomic analysis may improve our understanding of the mechanisms required for iron extraction in the presence of asbestos fibres and, more generally, of other metabolic pathways involved in asbestos weathering by *P. aeruginosa*.

Overall, we describe an original approach to improve the alteration of asbestos by bacteria. Given the major public health problem of asbestos and the lack of efficient waste management, this work demonstrates a low-energy and low-cost approach that could lead to a sustainable process that may have significant and beneficial societal repercussions. This strategy has the potential to be extended to other types of asbestos waste (such as asbestos cement) and more generally to bioleaching strategies (Williamson *et al*., 2021) for which the improvement of siderophore production may greatly improve the extraction capacity of bacteria.

Experimental procedures

Asbestos waste preparation

The flocking asbestos waste used in this study was obtained from the asbestos removal site of Jussieu University of Paris and kindly provided by the Mediterranean Company of Zeolites (SOMEZ). The asbestos waste consisted of chrysotile associated with a gypsum matrix. Asbestos samples (0.2 g) were sterilized by autoclaving (121°C for 20 min) and incubated at 70°C for 14 days before experimentation for complete sterilization of the material. Before experiments, samples were washed with 20 ml of sterile casamino acids medium without magnesium to remove free iron and magnesium.

Construction of the mutant PaM1

We chose to modify the promoter region of *pvdS* to render PVD production independent of iron. The promoter region was removed and replaced by the inducible promoter AraC/pBAD (Newman and Fuqua, 1999). Replacement of the promoter region was performed by

inserting the suicide vector carrying the substitution (pEXG2::AraC/pBAD*pvdS)* in the PAO1 strain, followed by homologous recombination. To construct the plasmid (pEXG2::AraC/pBAD*pvdS*), two regions of 700 pb flanking the promoter region of *pvdS* were PCR-amplified from genomic DNA with Phusion High-Fidelity DNA polymerase (Thermo Fisher Scientific, Waltham, MA, USA) using the primers pvdSam_F and pvdSam_R and pvdSav_F and pvdSav_R (Table S1). The promoter region of AraC/pBAD was amplified from plasmid pBAD24 using the primers pBad_F and pBad_R. Primers were designed to contain an additional 15 bp of homology with the end of the two amplified regions flanking the *pvdS* promoter. A fusion PCR was carried out to assemble the three fragments and reconstitute the substitution cassette. The cassette was then digested with EcoRI and XhoI (Thermo Fisher Scientific) and inserted by ligation into the plasmid pEXG2 (Rietsch *et al*., 2005) already digested with the same restriction enzymes to obtain the final plasmid pEXG2::AraC/pBAD*pvdS*. TOP10 cells were then transformed with this plasmid and used in triparental conjugation with *P. aeruginosa* PAO1 as the receiver strain and *E. Coli* HB101 (Boyer and Roulland-dussoix, 1969) as the helper strain. A two-step process allows allelic exchange between the vector and the chromosome mediated by homologous recombination (Hmelo *et al*., 2015). Briefly, for the triparental conjugation, the strains were grown overnight at 37°C without antibiotics and 500 μl of each culture was mixed and gently pelleted. The pellet was then resuspended in 50 μl of fresh Luria Bertani broth (LB)-rich medium and plated on an LB plate before incubating for 5 h at 37°C. The resulting biofilm-forming colony was recovered with an inoculation loop, resuspended in 1 ml LB, and 100 μl spread on LB plate with 30 μg ml^{-1} gentamycin (Gm) and 10 μg ml^{-1} chloramphenicol (Chl) to select for plasmid integration. After 2 days of incubation at 37°C, colonies were grown for 4 h in 1 ml LB broth, pelleted, resuspended in 50 μl fresh LB medium and streaked onto LB agar with 6% (w/v) sucrose for counter-selection to force plasmid excision. Colonies that lost Gm resistance were selected and the substitution was verified by PCR and sequencing (Eurofins genomic) using the primers pvdSam_F and pvdSav_R (Table S1).

Growth conditions and pyoverdine production

The two *P. aeruginosa* strains PAO1 and PaM1 were grown routinely for 24 h at 30°C in LB with shaking (220 rpm). To assess PVD production, pre-cultured cells were harvested and washed twice with sterile iron-poor CAA medium (composition in g l^{-1}: casamino acids 5, K_2HPO_4.3 H_2O 1.46, $MgSO_4$.7 H_2O 0.25) or rich Mueller Hinton medium (Becton Dickinson, Franklin Lakes, NJ, USA). After overnight culture, the cells were pelleted by centrifugation at 9871 *g* for 5 min, washed twice with sterile CAA or MH and adjusted to an OD_{600} of 0.05. The culture was optionally supplemented with arabinose (0.5% w/v) and/or $FeCl_3$ (for a final concentration of 5 μM $FeCl_3$). For the 24-h kinetic assays, the cell culture was performed in a 96-well U-bottom microplate at 30°C for 24 h. The bacterial density and PVD were measured directly with a TECAN microplate reader every 30 min at OD_{600} and OD_{400}, respectively, after a short orbital shaking of 10 s. For end-point experiments in 50-ml Falcon tubes, cultures were incubated in a shaker (220 rpm) at 30°C. After 24 h and 48 h of culture, the OD_{600} was measured in a spectrophotometer (Biophotometer Eppendorf). The OD_{400} of the supernatant was measured after centrifugation (5 min at 9871 *g*) of the culture (SPECORD 205 Analytik Jena). To measure iron and magnesium depletion from asbestos, cells from an LB-pre-culture were washed once in sterile CAA medium without magnesium (CAA(-Mg)). For bacterial suspensions, cells were washed once with sterile CAA(-Mg). The cell density was adjusted to an OD_{600} of 0.1, corresponding to 1–2 x 10^8 CFU ml^{-1}, and the cells diluted to obtain a starting inoculum between 6 x 10^4 and 1 x 10^5 CFU ml^{-1}. The culture was supplemented with arabinose (1%) in the presence or absence of FAW. Cultures were incubated for 24 h at 30°C with shaking (200 rpm).

Measurement of gene expression by RT-qPCR

Total RNA was extracted from mid-log phase bacterial cultures (OD_{600} = 0.5 to 1), after 8 h of incubation in CAA optionally supplemented with 5 μM $FeCl_3$ or 0.5% (w/v) arabinose, using the RNeasy MiniKit and QiaShredder columns (Qiagen, Hilden, Germany) according to the manufacturer's instructions. An additional double DNAse treatment was performed on the column and the eluate directly using RNase-Free DNase Set (Qiagen). A total of 1 μg of purified RNA was reverse-transcribed using the High-Capacity cDNA Reverse Transcription Kit (Applied Biosystems, Waltham, MA). The cDNA levels of the genes *pvdS, pvdD and pvdA* were measured using SYBR Green PCR Master Mix (Applied Biosystems, Step one plus real time PCR System) with appropriate primers (Table S1). The transcript levels of interest were normalized against that of the *uvrD* gene, used as an internal control (Jo *et al*., 2003; Jeannot *et al*., 2005) and expressed as the ratio to the mRNA expressed in strain PAO1 grown in CAA without supplementation. Gene expression values were calculated, using an improved version of the $2^{-\Delta\Delta Ct}$ method for quantitative real-time

polymerase chain reaction data analysis, from three independent experiments (Rao *et al*., 2013).

Alteration of flocking asbestos waste by Pseudomonas aeruginosa

To alter FAW, *Pseudomonas aeruginosa* strains PAO1 and PaM1 were cultured for five renewal cycles of 24 h at 30°C with shaking (220 rpm). Bacterial suspensions (20 ml), prepared in CAA(-Mg) as described previously, were added to FAW samples (0.2 g). Assays were performed in triplicate. Bacterial enumeration was performed at the end of every cycle by serial dilution-plating on LB agar and the plates were incubated at 30°C for 24 h. The 20-ml assays were then gently centrifuged for 5 min at 67 *g* to separate the bacterial cells from the asbestos fibres. An aliquot of 10 ml was removed and the remaining 10 ml diluted four times as follows: addition of 20 ml of sterile CAA(-Mg), centrifugation for 5 min at 67 *g* to separate the bacterial cells from the asbestos fibres and elimination of 20 ml of bacterial cells. Then, 10 ml of sterile CAA(-Mg) was added to perform a new cycle.

The iron and magnesium content in the cells and supernatants, as well as the amount of PVD in the supernatant were measured on the removed 10 ml, which were centrifuged for 10 min at 9871 *g* and the supernatant was filtered (0.22 μm porosity). Bacterial pellets were washed once with ultrapure water and dried at 50°C for 48 h. Dried pellets were mineralized by incubation in 77 μl 65% (v/v) HNO_3 for 48 h at room temperature. The volume was brought to 5 ml with ultrapure water to obtain 1% HNO_3 and the samples filtered through a membrane with a 0.22 μm filter unit. The iron and magnesium content were measured by colorimetric assay (see below) and the amount of PVD in solution in the supernatant was calculated from the absorbance at 400 nm using the extinction coefficients $\varepsilon = 19\,000$ (M) cm^{-1} (Meyer and Abdallah, 1978; Albrecht-Gary *et al*., 1994).

Iron and magnesium assay

The sensitive bathophenanthroline colorimetric method was used to determine the ferrous iron content of each sample (Baumann *et al*., 2019). The addition of thioglycolic acid converts ferric iron to ferrous iron to determine total iron content. Each sample was analysed in triplicate as follows: to each well of a 96-well plate (PS flat-bottom microplate, Greiner, San Jose, CA, USA), 20 μl of sample, 40 μl of saturated sodium acetate (5.5 M) (Sigma-Aldrich [Merck], Darmstadt, Germany), 80 μl of cold distilled water, 10 μl of thioglycolic acid (10% in distilled water) (Sigma-Aldrich) and 10 μl of bathophenanthroline (0.5% in distilled water) (Sigma-Aldrich) were added. After shaking, the microplates were stored overnight at 4°C. After shaking, the absorbance was measured at 535 nm using a Tecan microplate reader (Infinite 200 Pro; Tecan, Männedorf, Switzerland). Iron content (μg) was determined by comparing the values to a $FeCl_3$ standard reference curve. For magnesium content, the calmagite method was used (ELITech magnesium calmagite kit, San Jose, CA, USA). Ethylene glycol tetra acid (EGTA) was added to eliminate any interfering calcium, allowing calmagite to form a stable coloured complex with magnesium only. The reactive solution was prepared by mixing one volume of reagent 1 (1 M 2-methyl-2-amino-1-propanol and 215 μM EGTA) with one volume of reagent 2 (300 μM calmagite). Samples were analysed in triplicate in a 96-well plate (Greiner; PS flat-bottom microplate). In each well, 3 μl of sample were mixed with 300 μl of the reactive solution. After shaking and 30 s of incubation, the absorbance was measured at 500 nm using a Tecan microplate reader (Infinite 200 Pro; Tecan). Magnesium content (μg) was determined by comparing the values to a calibration curve established with known concentrations of $MgSO_4$.

STEM-EDX of asbestos fibres

TEM (Transmission Electron Microscopy) images were recorded with a JEOL 2100 microscope with a 200 kV potential applied to a LaB6 filament as an electron source. Resolution of the TEM was 0.21 nm. TEM mapping was performed in STEM (scanning transmission electron microscopy) mode (resolution 2 nm), using an SSD-EDX (silicon drift detector-energy dispersive X-ray) spectrometer to determine the chemical composition.

Statistical analysis

Results presented in all figures correspond to the mean values of three replicates. Significant statistical differences between values were determined using the Kruskal–Wallis test (R version 1.0.153), followed by a Conover post-hoc analysis. Results of the statistical analysis are given with letters: bars harbouring the same letter(s) are not significantly different, bar harbouring different letters are significantly different ($P \geq 0.05$).

Acknowledgements

This work has been conducted under the framework of the IdEx Unistra supported by the Investments for the future programme of the French Government and partially funded by the agence nationale de la Recherche. The authors thank the support of the French R&D plan for asbestos removal (PRDA) and SOMEZ (Mediterranean Company of Zeolites).

Conflict of interest

There are no conflicts of interest to declare.

References

Ahmed, E., and Holmström, S.J.M. (2014) Siderophores in environmental research: roles and applications. *J Microbial Biotechnol* **7:** 196–208.

Albelda-Berenguer, M., Monachon, M., and Joseph, E. (2019) Chapter Five - Siderophores: From natural roles to potential applications. In *Advances in Applied Microbiol*. Gadd, G.M., and Sariaslani, S. (eds). Cambridge, MA: Academic Press, pp. 193–225.

Albrecht-Gary, A.-M., Blanc, S., Rochel, N., Ocaktan, A.Z., and Abdallah, M.A. (1994) Bacterial iron transport: coordination properties of pyoverdin PaA, a peptidic siderophore of *Pseudomonas aeruginosa*. *Inorg Chem* **33:** 6391–6402.

Andrews, S.C., Robinson, A.K., and Rodríguez-Quiñones, F. (2003) Bacterial iron homeostasis. *FEMS Microbiol Rev* **27:** 215–237.

Aouad, G., Crovisier, J.-L., Damidot, D., Stille, P., Hutchens, E., Mutterer, J. *et al*. (2008) Interactions between municipal solid waste incinerator bottom ash and bacteria (*Pseudomonas aeruginosa*). *Sci Total Environ* **393:** 385–393.

Aznar, A., and Dellagi, A. (2015) New insights into the role of siderophores as triggers of plant immunity: what can we learn from animals? *J Exp Bot* **66:** 3001–3010.

Balzer, S., Kucharova, V., Megerle, J., Lale, R., Brautaset, T., and Valla, S. (2013) A comparative analysis of the properties of regulated promoter systems commonly used for recombinant gene expression in *Escherichia coli*. *Microb Cell Fact* **12:** 26.

Baumann, B.H., Shu, W., Song, Y., Sterling, J., Kozmik, Z., Lakhal-Littleton, S., and Dunaief, J.L. (2019) Liver-specific, but not retina-specific, hepcidin knockout causes retinal iron accumulation and degeneration. *Am J Pathol* **189:** 1814–1830.

Becker, F., Wienand, K., Lechner, M., Frey, E., and Jung, H. (2018) Interactions mediated by a public good transiently increase cooperativity in growing *Pseudomonas putida* metapopulations. *Sci Rep* **8:** 4093.

Bhattacharya, S., Ledwani, L., and John, P.J. (2016) Siderophores, the answer for micro to nanosized asbestos fibre related health hazard. 1724: 020102.

Boukhalfa, H., and Crumbliss, A.L. (2002) Chemical aspects of siderophore mediated iron transport. *Biometals Int J Role Met Ions Biol Biochem Med* **15:** 325–339.

Boyer, H.W., and Roulland-dussoix, D. (1969) A complementation analysis of the restriction and modification of DNA in *Escherichia coli*. *J Mol Biol* **41:** 459–472.

Braud, A., Geoffroy, V., Hoegy, F., Mislin, G.L.A., and Schalk, I.J. (2010) Presence of the siderophores pyoverdine and pyochelin in the extracellular medium reduces toxic metal accumulation in *Pseudomonas aeruginosa* and increases bacterial metal tolerance. *Environ Microbiol Rep* **2:** 419–425.

Budzikiewicz, H. (1997) Siderophores of fluorescent *Pseudomonads*. *Z Für Naturforschung C* **52:** 713–720.

Chen, Y., Jurkevitch, E., Bar-Ness, E., and Hadar, Y. (1994) Stability constants of pseudobactin complexes with transition metals. *Soil Sci Soc Am J* **58:** 390–396.

Cornelis, P., Wei, Q., Andrews, S.C., and Vinckx, T. (2011) Iron homeostasis and management of oxidative stress response in bacteria. *Metallomics* **3:** 540–549.

Cunrath, O., Geoffroy, V.A., and Schalk, I.J. (2016) Metallome of *Pseudomonas aeruginosa*: a role for siderophores. *Environ Microbiol* **18:** 3258–3267.

Daghino, S., Turci, F., Tomatis, M., Favier, A., Perotto, S., Douki, T., and Fubini, B. (2006) Soil fungi reduce the iron content and the DNA damaging effects of asbestos fibers. *Environ Sci Technol* **40:** 5793–5798.

David, S.R., Fritsch, S., Forster, A., Ihiawakrim, D., and Geoffroy, V.A. (2020) Flocking asbestos waste, an iron and magnesium source for *Pseudomonas*. *Sci Total Environ* **709:** 135936.

David, S.R., Ihiawakrim, D., Regis, R., and Geoffroy, V.A. (2020a) Efficiency of pyoverdines in iron removal from flocking asbestos waste: an innovative bacterial bioremediation strategy. *J Hazard Mater* **394:** 122532.

David, S.R., Ihiawakrim, D., Regis, R., and Geoffroy, V.A. (2020b) Iron removal from raw asbestos by siderophores-producing *Pseudomonas*. *J Hazard Mater* **385:** 121563.

Diep, P., Mahadevan, R., and Yakunin, A.F. (2018) Heavy metal removal by bioaccumulation using genetically engineered microorganisms. *Front Bioeng Biotechnol* **6:** 157.

Elmore, J.R., Furches, A., Wolff, G.N., Gorday, K., and Guss, A.M. (2017) Development of a high efficiency integration system and promoter library for rapid modification of *Pseudomonas putida* KT2440. *Metab Eng Commun* **5:** 1–8.

Ferret, C., Sterckeman, T., Cornu, J.-Y., Gangloff, S., Schalk, I.J., and Geoffroy, V.A. (2014) Siderophore-promoted dissolution of smectite by fluorescent *Pseudomonas*. *Environ Microbiol Rep* **6:** 459–467.

Fiche toxicologique Amiante (2018) *Fiche toxicologique amiante (No. 145)*. Paris, France: INRS.

Fuchs, R., Schafer, M., Geoffroy, V., and Meyer, J.-M. (2001) Siderotyping a powerful tool for the characterization of pyoverdines. *Curr Top Med Chem* **1:** 31–57.

Gasser, V., Guillon, L., Cunrath, O., and Schalk, I.J. (2015) Cellular organization of siderophore biosynthesis in *Pseudomonas aeruginosa*: evidence for siderosomes. *J Inorg Biochem* **148:** 27–34.

Groisman, E.A., Hollands, K., Kriner, M.A., Lee, E.-J., Park, S.-Y., and Pontes, M.H. (2013) Bacterial Mg^{2+} homeostasis, transport, and virulence. *Annu Rev Genet* **47:** 625–646.

Gull, M., and Hafeez, F.Y. (2012) Characterization of siderophore producing bacterial strain *Pseudomonas fluorescens* Mst 8.2 as plant growth promoting and biocontrol agent in wheat. *Afr J Microbiol Res* **6:** 6308–6318.

Hassan, H., and Troxell, B. (2013) Transcriptional regulation by Ferric Uptake Regulator (Fur) in pathogenic bacteria. *Front Cell Infect Microbiol* **3:** 59.

Hatzipantelis, E.S., Karasmanis, K., Perifanis, V., Vlachaki, E., Tziomalos, K., and Economou, M. (2014) Combined chelation therapy with deferoxamine and deferiprone in β-thalassemia major: compliance and opinions of young thalassemic patients. *Hemoglobin* **38:** 111–114.

Heldal, M., Norland, S., and Tumyr, O. (1985) X-ray microanalytic method for measurement of dry matter and

elemental content of individual bacteria. *Appl Environ Microbiol* **50:** 1251–1257.
Hmelo, L.R., Borlee, B.R., Almblad, H., Love, M.E., Randall, T.E., Tseng, B.S. *et al*. (2015) Precision-engineering the *Pseudomonas aeruginosa* genome with two-step allelic exchange. *Nat Protoc* **10:** 1820–1841.
Holden, V.I., and Bachman, M.A. (2015) Diverging roles of bacterial siderophores during infection. *Metallomics* **7:** 986–995.
Huse, H.K., Kwon, T., Zlosnik, J.E.A., Speert, D.P., Marcotte, E.M., and Whiteley, M. (2013) *Pseudomonas aeruginosa* enhances production of a non-alginate exopolysaccharide during long-term colonization of the cystic fibrosis lung. *PLOS One* **8:** e82621.
Jeannot, K., Sobel, M.L., El Garch, F., Poole, K., and Plésiat, P. (2005) Induction of the MexXY efflux pump in *Pseudomonas aeruginosa* is dependent on drug-ribosome interaction. *J Bacteriol* **187:** 5341–5346.
Jo, J.T.H., Brinkman, F.S.L., and Hancock, R.E.W. (2003) Aminoglycoside efflux in *Pseudomonas aeruginosa*: involvement of novel outer membrane proteins. *Antimicrob Agents Chemother* **47:** 1101–1111.
Johnstone, T.C., and Nolan, E.M. (2015) Beyond iron: non-classical biological functions of bacterial siderophores. *Dalton Trans* **44:** 6320–6339.
Josts, I., Veith, K., Normant, V., Schalk, I.J., and Tidow, H. (2021) Structural insights into a novel family of integral membrane siderophore reductases. *Proc Natl Acad Sci USA* **118:** e2101952118.
Kahlon, R. (2016) Biodegradation and bioremediation of organic chemical pollutants by *Pseudomonas*.
Kanarek, M.S. (2011) Mesothelioma from Chrysotile Asbestos: Update. *Ann Epidemiol* **21:** 688–697.
Khan, A., Singh, P., and Srivastava, A. (2018) Synthesis, nature and utility of universal iron chelator – Siderophore: a review. *Microbiol Res* **212–213:** 103–111.
Kraemer, S.M. (2004) Iron oxide dissolution and solubility in the presence of siderophores. *Aquat Sci* **66:** 3–18.
Leoni, L., Orsi, N., de Lorenzo, V., and Visca, P. (2000) Functional analysis of PvdS, an iron starvation sigma factor of *Pseudomonas aeruginosa*. *J Bacteriol* **182:** 1481–1491.
McPhee, J.B., Bains, M., Winsor, G., Lewenza, S., Kwasnicka, A., Brazas, M.D. *et al*. (2006) Contribution of the PhoP-PhoQ and PmrA-PmrB two-component regulatory systems to Mg^{2+}-induced gene regulation in *Pseudomonas aeruginosa*. *J Bacteriol* **188:** 3995–4006.
Meyer, J.M., and Abdallah, M.A. (1978) The fluorescent pigment of *Pseudomonas fluorescens*: biosynthesis, purification and physicochemical properties. *Microbiology* **107:** 319–328.
Meyer, J.-M., Gruffaz, C., Raharinosy, V., Bezverbnaya, I., Schäfer, M., and Budzikiewicz, H. (2008) Siderotyping of fluorescent *Pseudomonas*: molecular mass determination by mass spectrometry as a powerful pyoverdine siderotyping method. *Biometals Int J Role Met Ions Biol Biochem Med* **21:** 259–271.
Miethke, M., and Marahiel, M.A. (2007) Siderophore-based iron acquisition and pathogen control. *Microbiol Mol Biol Rev* **71:** 413–451.
Mislin, G.L.A., and Schalk, I.J. (2014) Siderophore-dependent iron uptake systems as gates for antibiotic Trojan horse strategies against *Pseudomonas aeruginosa*. *Met Integr Biometal Sci* **6:** 408–420.
Mohanty, S.K., Gonneau, C., Salamatipour, A., Pietrofesa, R.A., Casper, B., Christofidou-Solomidou, M., and Willenbring, J.K. (2018) Siderophore-mediated iron removal from chrysotile: implications for asbestos toxicity reduction and bioremediation. *J Hazard Mater* **341:** 290–296.
Newman, J.R., and Fuqua, C. (1999) Broad-host-range expression vectors that carry the L-arabinose-inducible *Escherichia coli* araBAD promoter and the araC regulator. *Gene* **227:** 197–203.
Nikel, P.I., Chavarría, M., Danchin, A., and de Lorenzo, V. (2016) From dirt to industrial applications: *Pseudomonas putida* as a Synthetic Biology chassis for hosting harsh biochemical reactions. *Curr Opin Chem Biol* **34:** 20–29.
Nosrati, R., Dehghani, S., Karimi, B., Yousefi, M., Taghdisi, S.M., Abnous, K. *et al*. (2018) Siderophore-based biosensors and nanosensors; new approach on the development of diagnostic systems. *Biosens Bioelectron* **117:** 1–14.
Ochsner, U.A., Johnson, Z., Lamont, I.L., Cunliffe, H.E., and Vasil, M.L. (1996) Exotoxin A production in *Pseudomonas aeruginosa* requires the iron-regulated *pvdS* gene encoding an alternative sigma factor. *Mol Microbiol* **21:** 1019–1028.
Paolini, V., Tomassetti, L., Segreto, M., Borin, D., Liotta, F., Torre, M., and Petracchini, F. (2019) Asbestos treatment technologies. *J Mater Cycles Waste Manag* **21:** 205–226.
Pascolo, L., Gianoncelli, A., Schneider, G., Salomé, M., Schneider, M., Calligaro, C. *et al*. (2013) The interaction of asbestos and iron in lung tissue revealed by synchrotron-based scanning X-ray microscopy. *Sci Rep* **3:** 1123.
Pasqua, M., Visaggio, D., Lo Sciuto, A., Genah, S., Banin, E., Visca, P., and Imperi, F. (2017) Ferric uptake regulator fur is conditionally essential in *Pseudomonas aeruginosa*. *J Bacteriol* **199:** e00472–e00417.
Petrik, M., Zhai, C., Haas, H., and Decristoforo, C. (2017) Siderophores for molecular imaging applications. *Clin Transl Imaging* **5:** 15–27.
Pohl, E., Haller, J.C., Mijovilovich, A., Meyer-Klaucke, W., Garman, E., and Vasil, M.L. (2003) Architecture of a protein central to iron homeostasis: crystal structure and spectroscopic analysis of the ferric uptake regulator. *Mol Microbiol* **47:** 903–915.
Qiu, D., Damron, F.H., Mima, T., Schweizer, H.P., and Yu, H.D. (2008) PBAD-based shuttle vectors for functional analysis of toxic and highly regulated genes in *Pseudomonas* and *Burkholderia* spp. and other bacteria. *Appl Environ Microbiol* **74:** 7422–7426.
Rajkumar, M., Vara Prasad, M.N., Freitas, H., and Ae, N. (2009) Biotechnological applications of serpentine soil bacteria for phytoremediation of trace metals. *Crit Rev Biotechnol* **29:** 120–130.
Rao, X., Huang, X., Zhou, Z., and Lin, X. (2013) An improvement of the 2ˆ(−delta delta CT) method for quantitative real-time polymerase chain reaction data analysis. *Biostat Bioinforma Biomath* **3:** 71–85.
Rietsch, A., Vallet-Gely, I., Dove, S.L., and Mekalanos, J.J. (2005) ExsE, a secreted regulator of type III secretion genes in *Pseudomonas aeruginosa*. *Proc Natl Acad Sci* **102:** 8006–8011.
Ringel, M.T., Dräger, G., and Brüser, T. (2018) PvdO is required for the oxidation of dihydropyoverdine as the last

step of fluorophore formation in *Pseudomonas fluorescens*. *J Biol Chem* **293:** 2330–2341.
Saha, M., Sarkar, S., Sarkar, B., Sharma, B.K., Bhattacharjee, S., and Tribedi, P. (2016) Microbial siderophores and their potential applications: a review. *Environ Sci Pollut Res Int* **23:** 3984–3999.
Saisho, Y., Katsube, T., White, S., Fukase, H., and Shimada, J. (2018) Pharmacokinetics, safety, and tolerability of cefiderocol, a novel siderophore cephalosporin for gram-negative bacteria, in healthy subjects. *Antimicrob Agents Chemother* **62:** e02163–e02117.
Schalk, I.J. (2018) A trojan-horse strategy including a bacterial suicide action for the efficient use of a specific gram-positive antibiotic on gram-negative bacteria. *J Med Chem* **61:** 3842–3844.
Schalk, I.J., Hannauer, M., and Braud, A. (2011) New roles for bacterial siderophores in metal transport and tolerance. *Environ Microbiol* **13:** 2844–2854.
Schalk, I.J., Rigouin, C., and Godet, J. (2020) An overview of siderophore biosynthesis among fluorescent *Pseudomonads* and new insights into their complex cellular organization. *Environ Microbiol* **22:** 1447–1466.
Scherpereel, A. (2016) Amiante et pathologie respiratoire. *Presse Médicale* **45:** 117–132.
Serrano, L.O.D. (2017) Biotechnology of siderophores in high-impact scientific fields. *Biomol Concepts* **8:** 169–178.
Spasiano, D., and Pirozzi, F. (2017) Treatments of asbestos containing wastes. *J Environ Manage* **204:** 82–91.
Tonziello, G., Caraffa, E., Pinchera, B., Granata, G., and Petrosillo, N. (2019) Present and future of siderophore-based therapeutic and diagnostic approaches in infectious diseases. *Infect Dis Rep* **11:** 8208.
Upritchard, H.G., Yang, J., Bremer, P.J., Lamont, I.L., and McQuillan, A.J. (2007) Adsorption to metal oxides of the *Pseudomonas aeruginosa* siderophore pyoverdine and implications for bacterial biofilm formation on metals. *Langmuir ACS J Surf Colloids* **23:** 7189–7195.
Valko, M., Jomova, K., Rhodes, C.J., Kuča, K., and Musílek, K. (2016) Redox- and non-redox-metal-induced formation of free radicals and their role in human disease. *Arch Toxicol* **90:** 1–37.
Venturi, V., Ottevanger, C., Bracke, M., and Weisbeek, P. (1995) Iron regulation of siderophore biosynthesis and transport in *Pseudomonas putida* WCS358: involvement of a transcriptional activator and of the Fur protein. *Mol Microbiol* **15:** 1081–1093.
Virta, R. (2002) *Asbestos: Geology, Mineralogy, Mining, and Uses*. Reston, VA: U.S. Geological Survey.
Wallis, S.L., Emmett, E.A., Hardy, R., Casper, B.B., Blanchon, D.J., Testa, J.R. *et al*. (2020) Challenging global waste management – bioremediation to detoxify asbestos. *Front Environ Sci* **8:** 20.
Wilderman, P.J., Vasil, A.I., Johnson, Z., Wilson, M.J., Cunliffe, H.E., Lamont, I.L., and Vasil, M.L. (2001) Characterization of an endoprotease (PrpL) encoded by a PvdS-regulated gene in *Pseudomonas aeruginosa*. *Infect Immun* **69:** 5385–5394.
Williamson, A.J., Folens, K., Matthijs, S., Cortez, Y.P., Varia, J., Laing, G.D. *et al*. (2021) Selective metal extraction by biologically produced siderophores during bioleaching from low-grade primary and secondary mineral resources. *BioRxiv* **163:** 106774.
Zobel, S., Benedetti, I., Eisenbach, L., de Lorenzo, V., Wierckx, N., and Blank, L.M. (2015) Tn7-based device for calibrated heterologous gene expression in *Pseudomonas putida*. *ACS Synth Biol* **4:** 1341–1351.

Supporting information

Additional supporting information may be found online in the Supporting Information section at the end of the article.

Appendix S1

Fig. S1. Bacterial growth (OD600) of *P. aeruginosa* strains PAO1 (A) and PaM1 (B) in the presence of increasing arabinose concentrations (0.01 to 0.5% (v/v)).

Fig. S2. Bacterial growth (OD600) of *P. aeruginosa* strains PAO1 (A) and PaM1 (B) strains in the presence of increasing iron ($FeCl_3$) concentrations (50 nM to 50 μM).

Fig. S3. Amount of PVD relative to the growth of *P. aeruginosa* strains PAO1 (grey bars) and PaM1 (white bars). The relative amount was assessed during five growth cycles of 24 h in CAA medium without magnesium CAA(-Mg) supplemented with arabinose, in the presence (dots) or absence of flocking asbestos waste (plain). Error bars indicate the standard errors of the means of three biological replicates.

Fig. S4. STEM images and STEM mapping of chrysotile fibers from flocking asbestos waste after five growth cycles of 24 h in the presence of PAO1 (A and C) or PaM1 (B and D). Large images obtained by combining the distributions of Mg, Si, and Fe, with analysis areas (A and B). Atomic ratios of Mg/Si and Fe/Si of various areas (C and D) and the total area (F). Mass percentage of Mg, Si, and Fe after growth cycles in the presence of PAO1 or the PaM1 (E).

Table S1. Primers used in this study.

